Electronic Supplementary Material (ESI) for Journal of Materials Chemistry C.

Supporting Information

for

Prospects for experimental realization of two-dimensional aluminium allotropes

by

Igor Lukačević, Maja Varga Pajtler, Matko Mužević, Sanjeev K. Gupta

Supporting information (SI1)

There are no reference points on the structural properties of aluminene available for comparison. For example, we couldn't know the starting point for the buckling height of β-Al. On the other side, profound difference between the bulk structure of aluminium and conjectured monolayer structures of aluminene prevent us to assume the lattice parameters. Therefore, before using Broyden-Fletcher-Goldfarb-Shano (BFGS) minimization algorithm[1] to fully relax the β-Al structure (as well as the others), we first calculated the total energy as a function of both the lattice constant and the buckling height. As seen in Figure S1a, the best starting lattice constant and buckling height would be around 2.7 and 2.5 Å, respectively.

Similar procedure was used for γ_2-Al (Figures S1b-S1d).

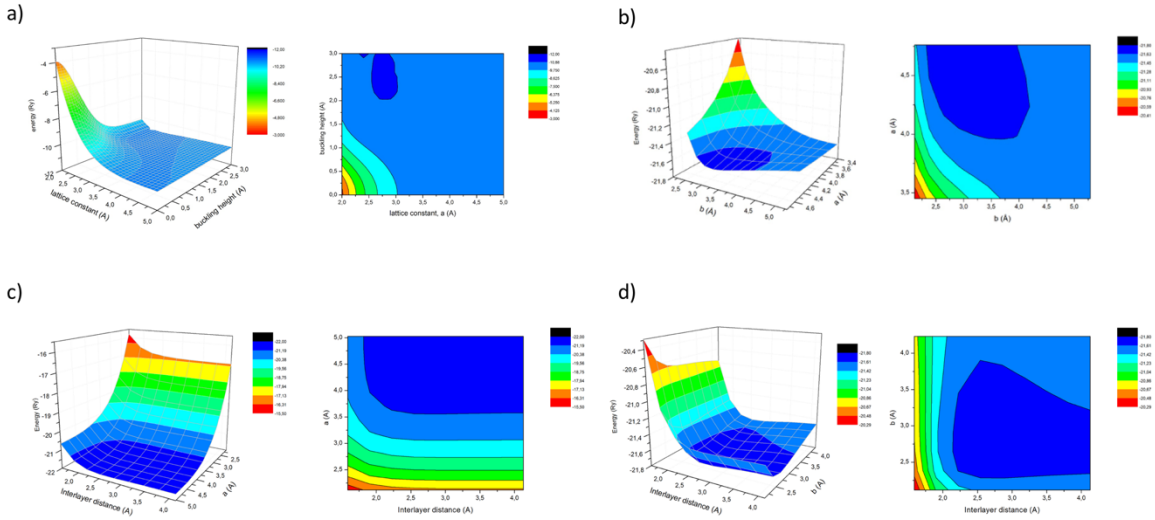

Figure S1. (a) Total energy dependence on the lattice constant and the buckling height in β-Al. (b)-(d) Total energy dependence on the lattice constants and the interlayer distance in γ_2-Al. Total energy is coloured coded in figure legends, with the lowest one represented with dark blue.

Supporting information (SI2)

At relevant strains the total energy of the studied structures retains its concave shape, indicating energy stability of the structures under both compressive and tensile strains in both armchair and zig-zag directions (Figure S2 left).

Curiously, at high compressive strains in armchair direction atoms in α-Al stop to separate and their relative distance remains constant (Figure S2 right). This event corresponds to the 'kink' (or appearance of another local energy minimum) in the total energy curve (Figure S2 left) at high compressive strains above -20%. This may indicate a structural phase transition caused by the external pressure upon the monolayer. It is questionable whether this event would have any physical meaning since α-Al is not dynamically stable at compressive strains.

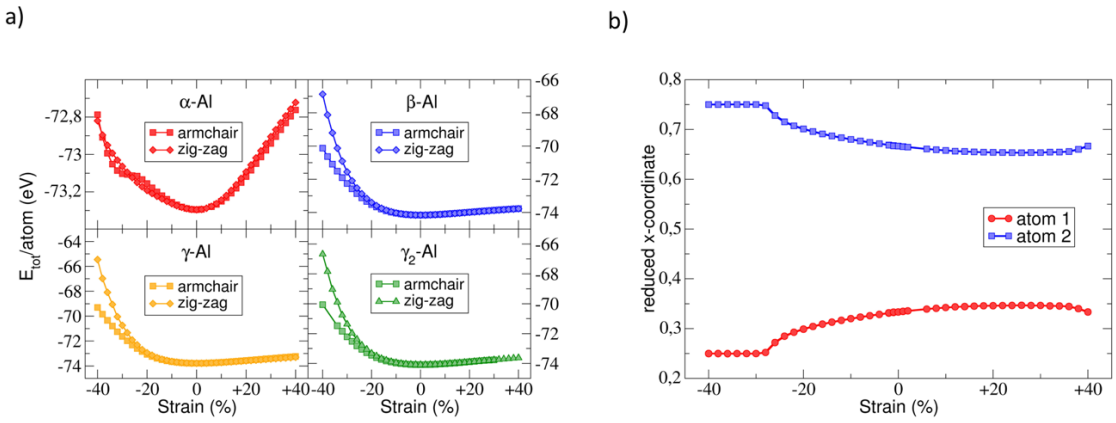

Figure S2. (a) Total energy dependence on the armchair and zig-zag uniaxial strains in α-Al, β-Al, γ-Al and γ_2-Al. Convex shape of the total energy around the energy minimum corresponds to the stability of the studied structures with respect to macroscopic deformation. (b) Variation of the atomic x-coordinate in α-Al with compressive and tensile strain in armchair direction.

Supporting information (SI3)

To support the conclusion that the studied monolayer structures are mechanically stable under the studied range of strains, we also calculated the strain energy, defined as an energy difference between the strained and the unstrained structure. Figure S3 gives the strain energy as a function of applied compressive or tensile strain. Strain energy behaves monotonously in the respective compressive and tensile strain ranges between -20% and +20%, which is the range of strains which we considered in our work. This behaviour implies that after the initial elastic deformation (within the range between -20% and +20%) is released, the structure would be restored to its starting state.[2]

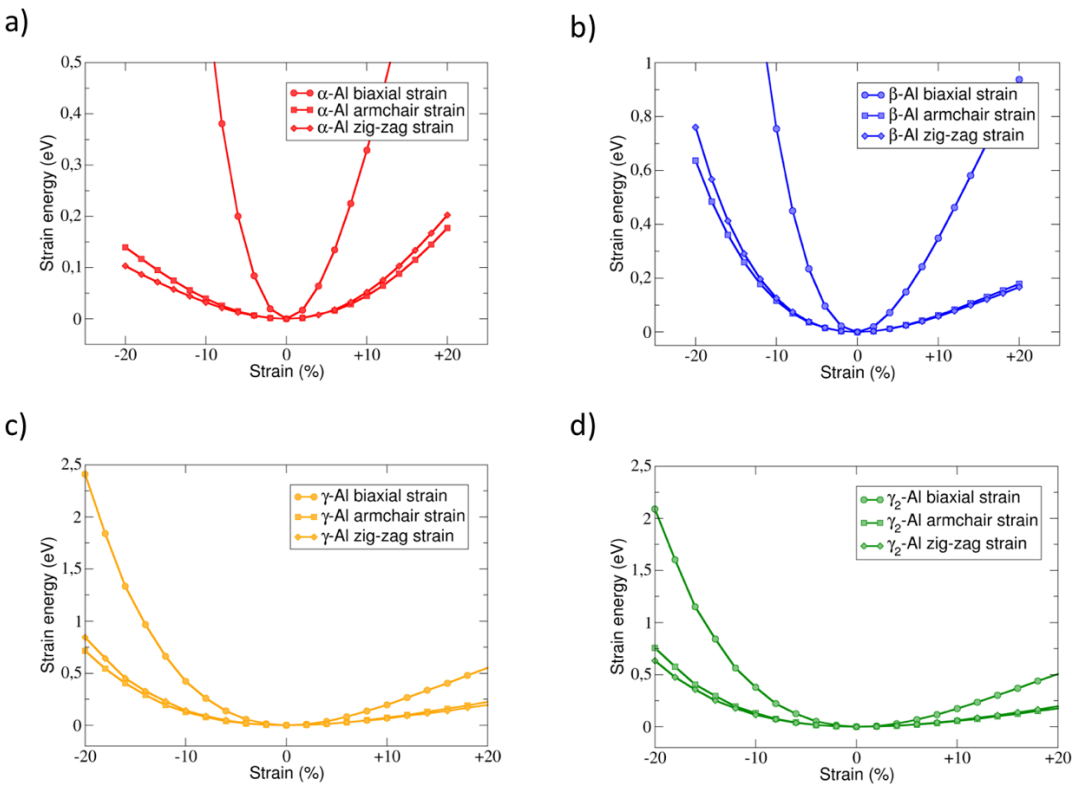

Figure S3. Strain energy of (a) α-Al, (b) β-Al, (c) γ-Al and (d) γ_2-Al as a function of applied compressive (negative) or tensile (positive) strain.

Supporting information (SI4)

Stress-strain relations with respect to different strains can reveal information on the elastic boundaries of a material. The strains corresponding to the highest achievable tensile stress ('ideal strength') is usually termed 'critical strain'. As can be seen from our results (Figure S4), biaxial critical strains are lower than the uniaxial ones. This is because biaxial strains change the strain energy much more rapidly and bring the materials structure faster to its elastic boundary. In our calculations, biaxial critical strains can all be found bellow 16%, while the uniaxial ones rise up to 40% (this was the limit we set in our calculations).

Difference between the critical strains in armchair and zig-zag directions points to the elastic anisotropy in aluminene. However, these differences are not large as in, for example, antimonene (puckered α-Sb),[3] but are similar to the ones in phosphorene (2D black phosphorus).[4] Therefore, the studied aluminene allotropes do show some measure of elastic anisotropy, with the smallest one found in α-Al. On the other hand, large critical strains found for zig-zag strains in β-Al, γ-Al and γ_2-Al could provide necessary elasticity for future strain engineering of electric or thermal properties of ultra-thin aluminium.

We have to mention here that in some calculations on γ_2-Al we could not converge the stress on the crystal lattice, irrespective of the calculation parameters, in the cases of biaxial (over 20%) and armchair (over 26%) strain directions. For higher strains, stress would oscillate. It is possible that other local minima exist with almost the same energies (with difference smaller that the calculation convergence criteria). During the relaxation, algorithm converges toward different atomic positions regarding the changes in the unit cell dimensions. Therefore, these data are missing in Figure S4 as well as in Figure 2. Also, after 30% stress is more or less constant. We, therefore, ascribed the critical strain to 30%, as it is less likely that the structure could endure larger strains.

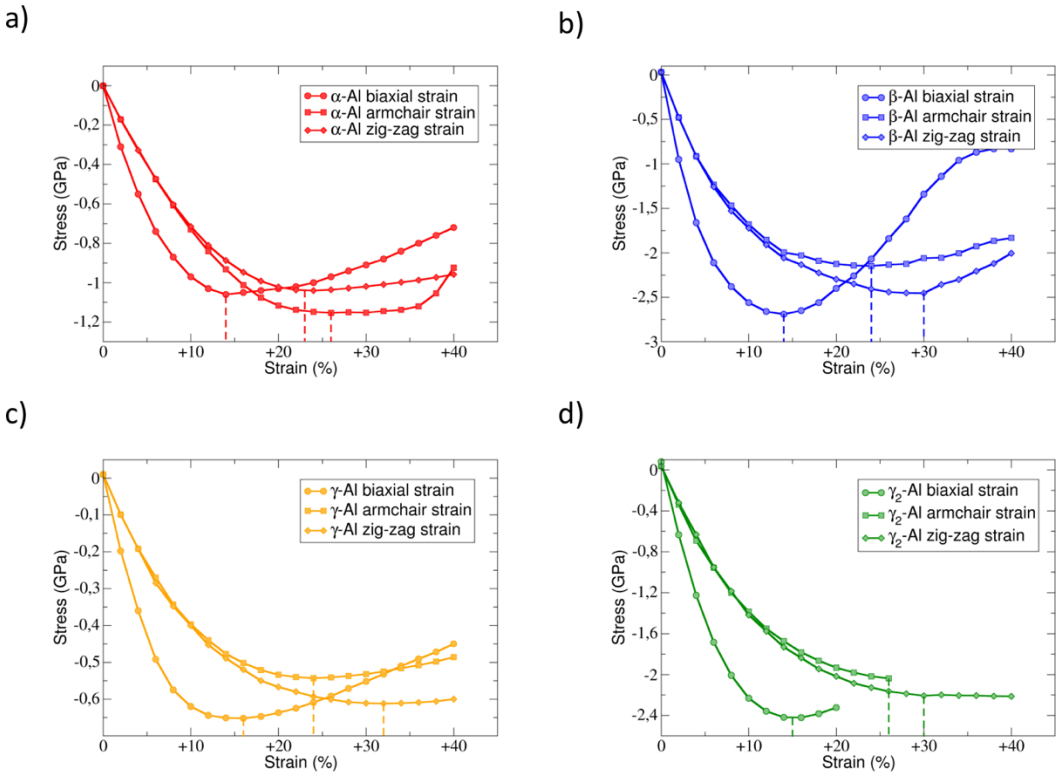

Figure S4. Stress-strain relations in α-Al, β-Al, γ-Al and γ_2-Al for both biaxial and uniaxial (armchair and zig-zag) strains. Changes in the behaviour of stress functions give the critical strains and are shown by dashed lines.

Supporting information (SI5)

Buckling height in β-Al decreases with the tensile strain (Figure S5). Expectedly, for biaxial strain it decreases much faster at larger strains. On the other hand, the critical biaxial strain occurs much earlier than the uniaxial ones, giving in the end about the same buckling height at the respective critical strain. It drops down from 2.44 Å to 2.26 Å at the critical biaxial strain of 14%. Uniaxial strains decrease the buckling height to 2.29 Å (armchair at the critical strain of 24%) and to 2.25 Å (zig-zag at the critical strain of 24%). These are the changes of 7%, 6% and 8% for the biaxial, armchair and zig-zag strains, respectively. Evidently, β-Al remains in its high buckled geometry. These changes are too small to remove the coupling of 'out-of-plane' and 'in-plane' phonon modes. Even strained up to its limits, β-Al preserves unstable lattice dynamics.

Phonon dispersion curves show that besides the unstable flexural acoustic mode, another 'in-plane' acoustic mode becomes unstable. Combined motion of atoms in these unstable phonon modes would eventually lead to the breaking apart the aluminene structure. Similar effect has been already predicted by *ab initio* calculations in high buckled silicene and germanene.[5]

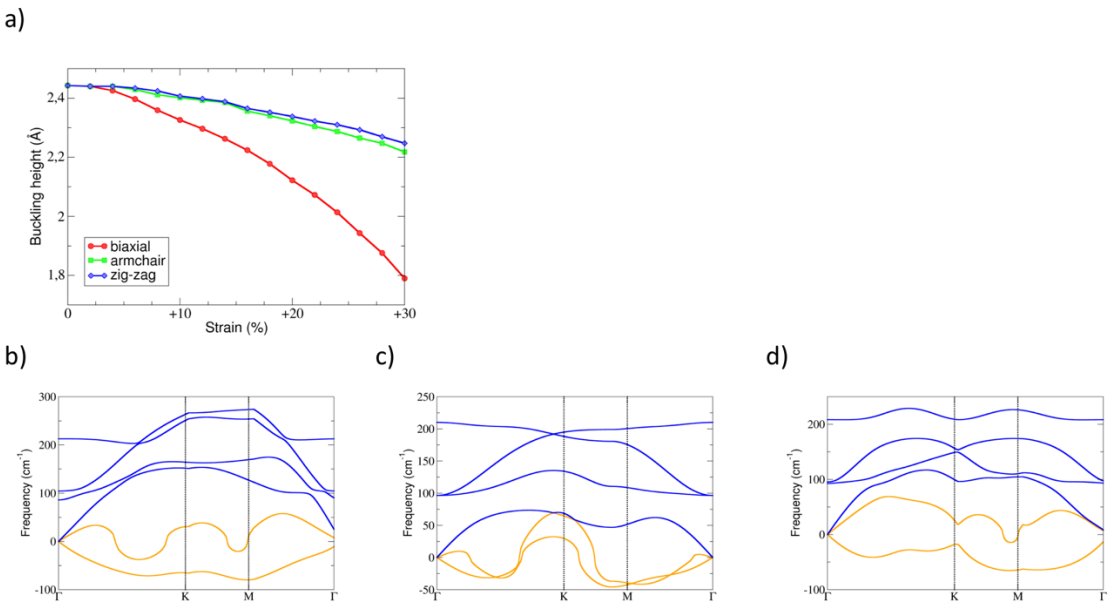

Figure S5. (a) Buckling height of β-Al for different tensile strains (up to the critical limit) and strain directions. Full phonon dispersion curves of β-Al at critical (b) biaxial, (c) armchair and (d) zig-zag strain. Unstable phonon modes are coloured in orange.

Supporting information (SI6)

Side view of β-Al relaxed on top of Cu(111) reveals the influence of the metallic substrate. Buckling height drops to zero and β-Al conforms to the planar geometry of α-Al, due both to the tensile strain and suppression of the buckling motion of atoms. Phonon dispersions of β-Al on Cu(111) are identical to the ones of α-Al on Cu(111) as expected from the above discussion.

On Cu(111) γ_2-Al relaxes to the triangular structure. However, the strain imposed by the substrate is not adequate to ensure the stability of phonon modes.

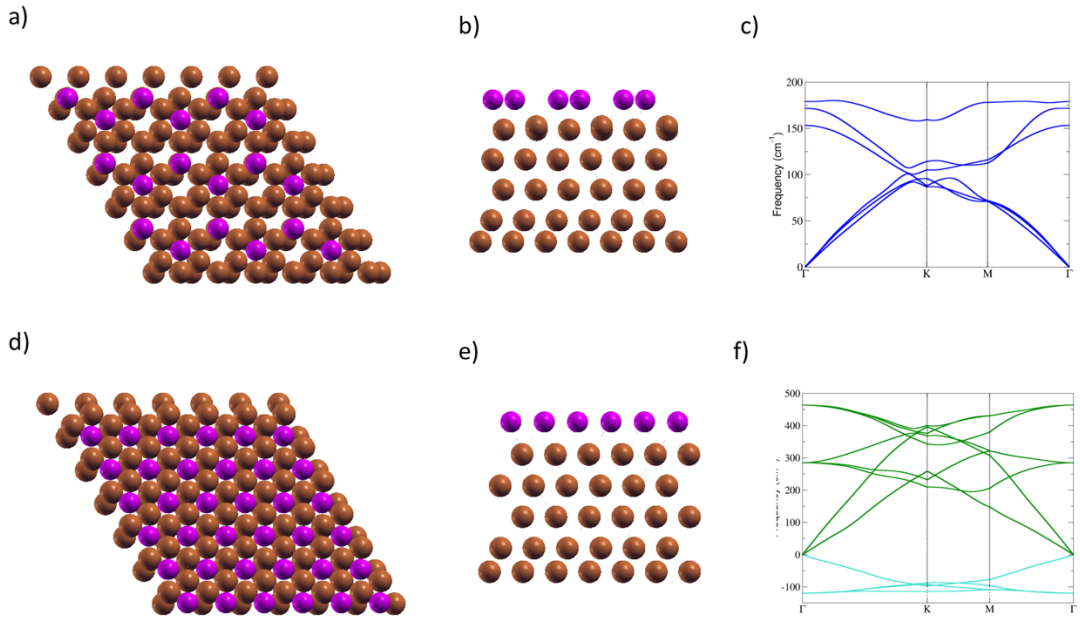

Figure S6. β-Al relaxed on top of Cu(111): (a) top and (b) side views along with (c) full phonon dispersion curves. γ_2-Al relaxed on top of Cu(111): (d) top and (e) side views along with (f) full phonon dispersion curves. Unstable phonon modes are coloured in turquoise.

Supporting information (SI7)

The strain induced on the aluminene monolayer by the substrate surface can be reproduced from the changes in the bond lengths. From the relaxation calculations under different strains one can obtain the bond lengths as the functions of strain. Upon relaxation of α-Al on Cu(111) we found that the bond length increases from 2.57 Å to 2.95 Å. Using the inverse of the above function, one can find the corresponding strain (Figure S7). It is found to be 14%, which falls in the segment of tensile biaxial strains for which α-Al has stable lattice dynamics (Figure 2c and S4).

Similar situation is predicted for α-Al on graphene (Figure S7). Bond length increases from 2.57 Å to 2.84 Å, which corresponds to the tensile strain of 10%, again inside the segment of biaxial strains with stable lattice dynamics.

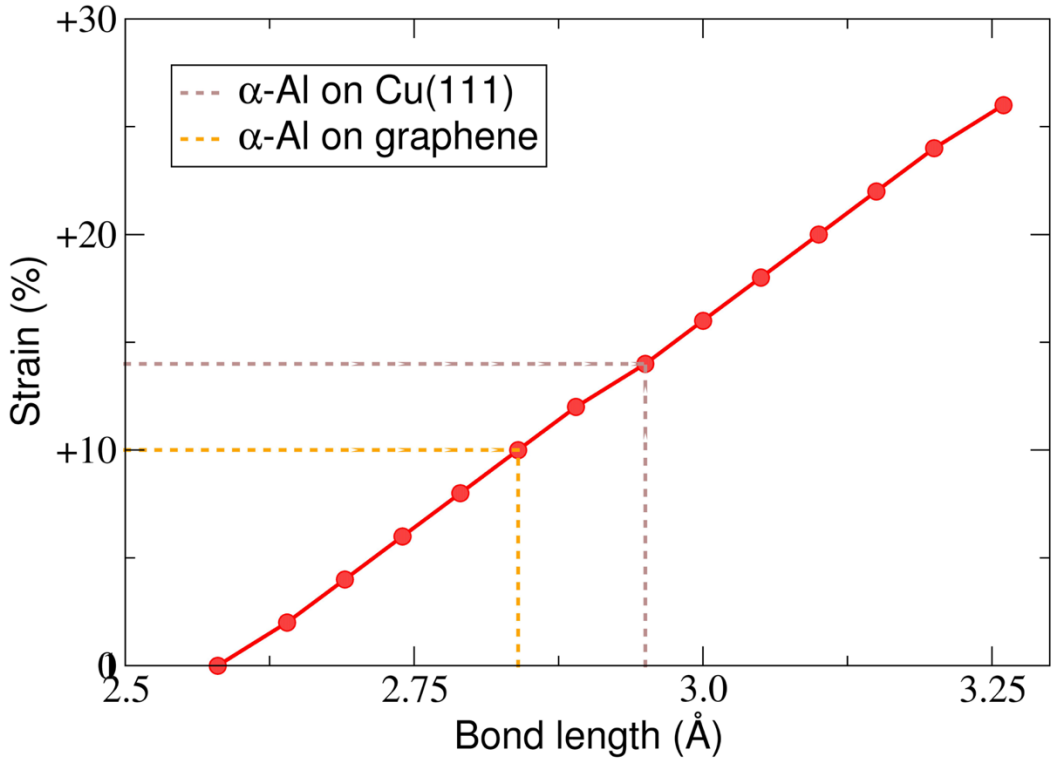

Figure S7. Bond lengths of α-Al relaxed on Cu(111) surface (brown dash lines) and unsupported graphene (orange dashed lines) with the corresponding induced strains.

Supporting information (SI8)

During the molecular dynamics relaxation of α-Al on Cu(111) and graphene substrates, we noticed negligibly small changes in time steps of 1 ps. Therefore, we chose to substantially increase the number of steps in order to verify that no thermal effects will break forth on a larger time scale (up to 1 ns). After that, small changes could be observed on the time scale of hundreds of picoseconds (Figure S8a and Supplementary videos SV1 and SV2). The intensity of these changes is insufficient to perturb the structure of aluminene and aluminene shows thermal stability at room temperature. At 400 K the structure of α-Al is still stable (not shown here).

As the time scale of atomic vibrations could be sub-picosecond, an additional proof of thermal stability can be obtained using shorter time steps in molecular dynamics simulations. Thus, we conducted the simulations with the time steps of 1 and 50 femtoseconds (with the total simulation times of 50 and 1000 femtoseconds, respectively) and plotted the radial distribution functions, g(r), of α-Al on Cu(111) and graphene substrates (Figure S8b). Visual inspection of the relaxation shows no changes in atomic positions, while radial distribution functions show clear sharp peaks belonging to the well-defined crystal structure of aluminene. These peaks correspond to the nearest neighbour distances of aluminium atoms. Small deviations are observed due to the thermal motion of atoms around the equilibrium positions. Additional broader peaks correspond to the Al-Cu, Al-C, Cu-Cu and C-C distances. We observe no changes in radial distribution functions when we decrease the simulation step time from 50 fs to 1 fs.

In order to assess the influence of structural defects on the stability of aluminene, we constructed a single-defect aluminene structure using the supercell approach. This systematic approach included 4 supercells with increasing sizes, from 1×1 to 4×4. Larger supercells are unfeasible for the current available computational resources. Then we conducted again the MD simulations at 300 K temperature and plotted the radial distribution functions (Figure S8c). As can be seen the radial distribution functions show sharp peaks, which correspond to the single-phase crystal structure. Low value peaks are not seen in the defect structures as nearest-neighbour distances are perturbed by the defect positions. Therefore, we can conclude that the aluminene structure is stable with respect to the single structural defect.

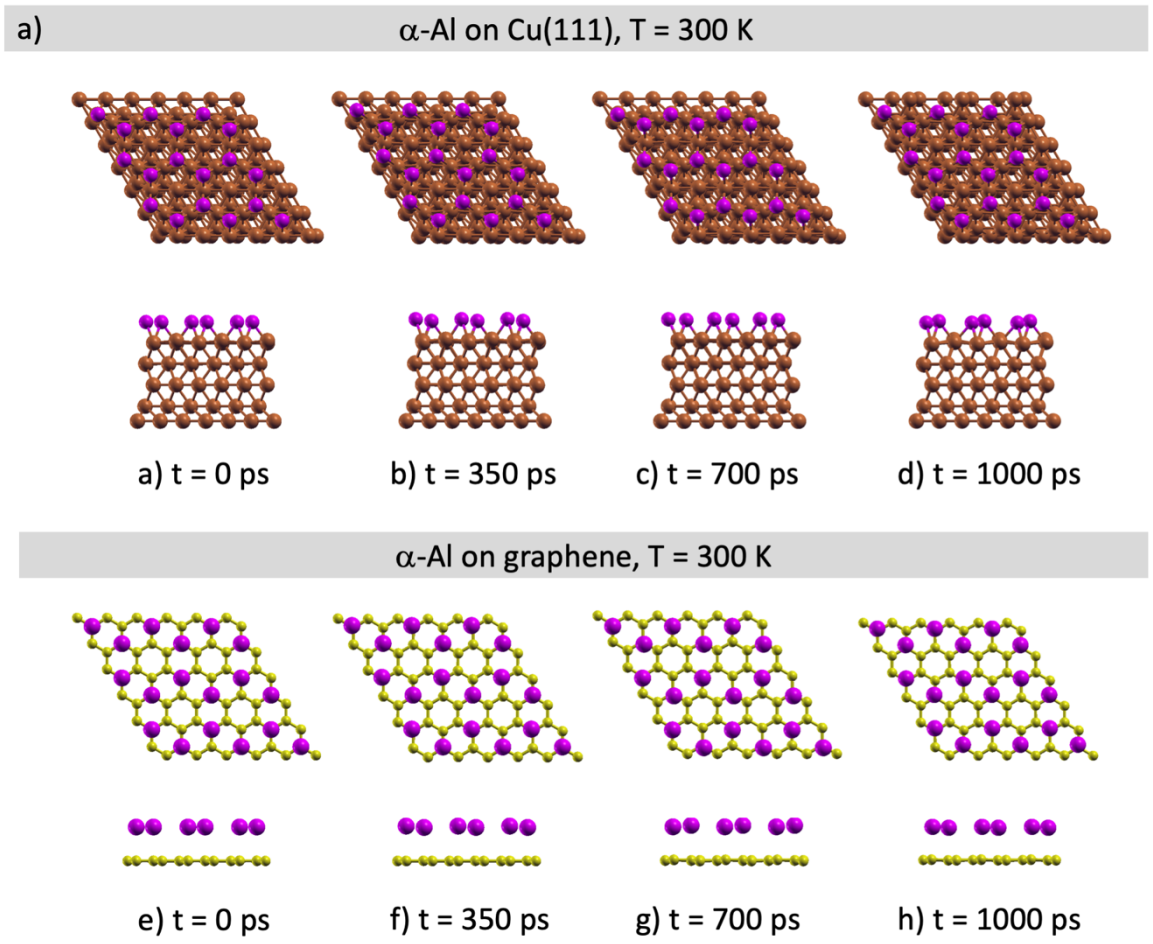
a)
α-Al on Cu(111), T = 300 K
a) t = 0 ps
b) t = 350 ps
c) t = 700 ps
d) t = 1000 ps
α-Al on graphene, T = 300 K
e) t = 0 ps
f) t = 350 ps
g) t = 700 ps
h) t = 1000 ps

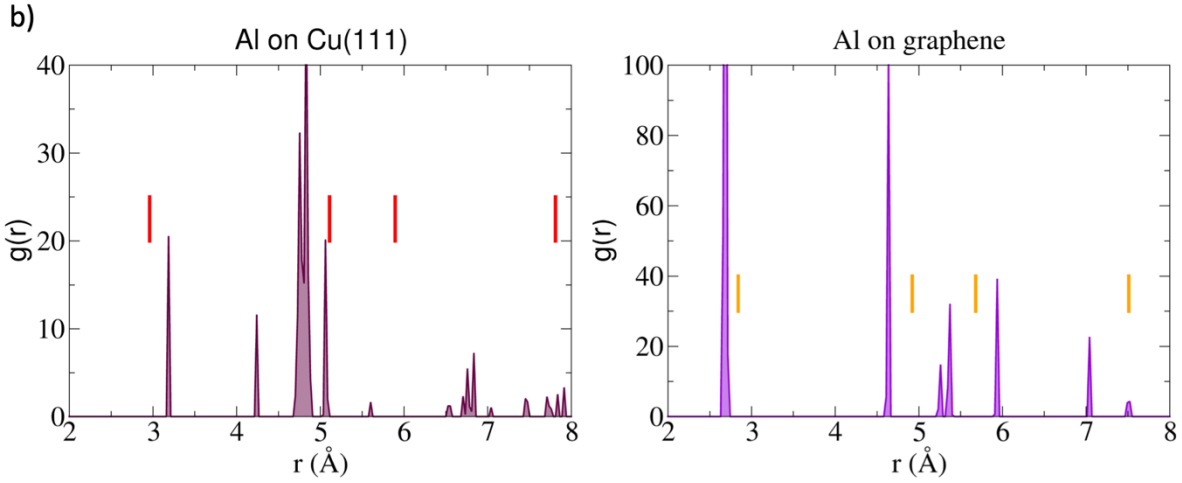
b)
Al on Cu(111)
g(r)
r (Å)
Al on graphene
g(r)
r (Å)

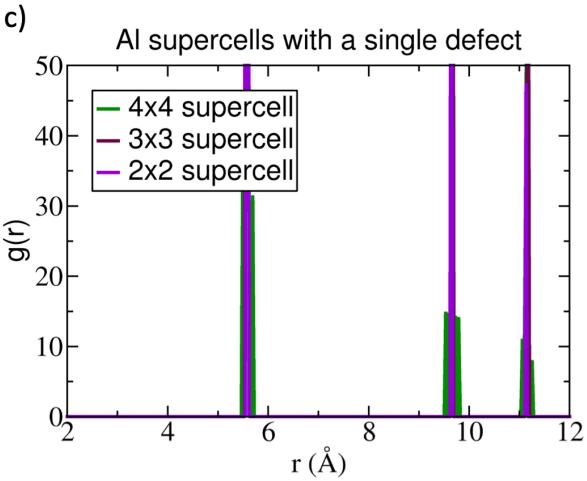

Figure S8. (a) Structure of α-Al on Cu(111) and graphene substrates at room temperature (T = 300 K) from *ab initio* molecular dynamics. Images show the structure at four different time steps up to 1 ns (= 1000 ps). Al atoms are coloured in violet, copper in orange and graphene in yellow. Both substrates yield stable aluminene at room temperature. (b) Radial distribution function, g(r), of α-Al on Cu(111) and graphene substrates at room temperature (T = 300 K) from *ab initio* molecular dynamics with time step of 1 fs. Red and orange lines show the first-, second-, third- and fourth-nearest neighbour distances. (c) Radial distribution function, g(r), of α-Al supercells (from 1×1 to 4×4) with a single-defect point at room temperature (T = 300 K) from *ab initio* molecular dynamics with time step of 1 fs. Peaks for different supercells overlap as there are no changes in g(r) with increasing supercell size.

Supporting information (SI9)

Local energy difference, E_{led}, is calculated as a difference between the total energy of a single adsorbed atom with the substrate and the total energy of the substrate without the adsorbate: $E_{led} = E_{atom+substrate} - E_{substrate}$. E_{led} is calculated for multiple localities at which the adsorbing atom could be found during the surface diffusion along the substrate surface. This process could approximate the chemical deposition routes and movements of atoms under thermal effects.

We chose five sites with different symmetries. At low-hcp site (l-hcp) Al atom is above the hole in the hcp structure of Cu(111). It is the position with the lowest energy, obtained through the structural relaxation of aluminium atoms on Cu(111). At high-hcp site (h-hcp) Al atom is found above the copper atom in the second sublayer of the Cu surface. Consequently, this site has the highest energy. Between these two sites, we chose the bridging position where Al atom is found over the Cu-Cu bond in the hcp hexagon of the first surface layer. Other two sites are transition sites which correspond to the mid-positions between the above-mentioned ones.

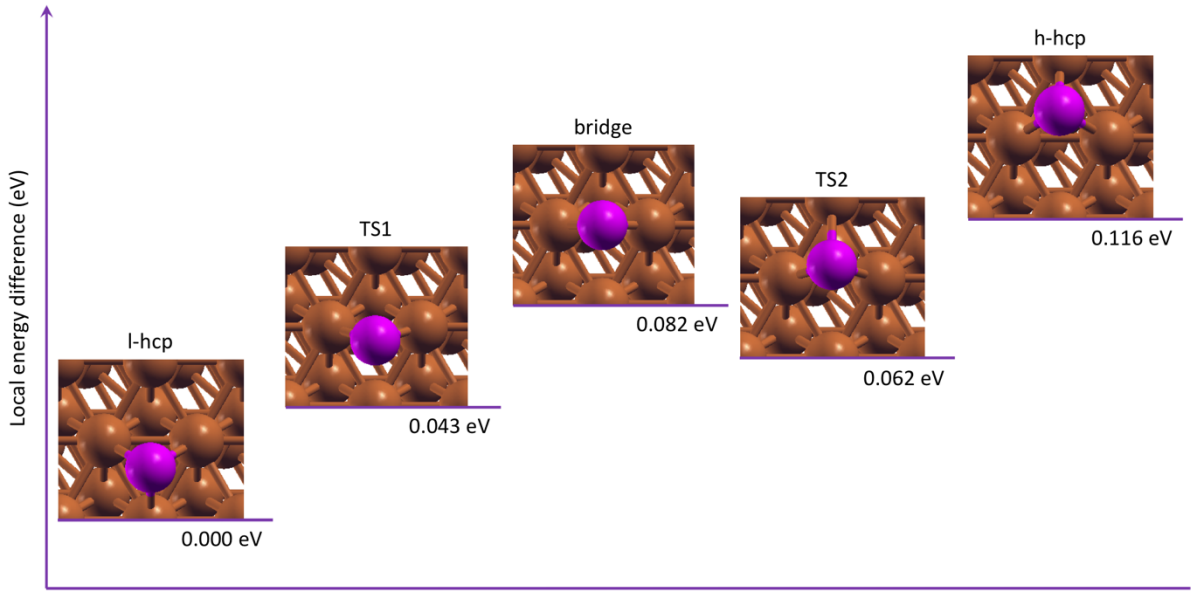

Figure S9. Local energy difference of aluminium atoms at different sites on Cu(111) surface: low-hcp site (l-hcp), transition sites (TS 1 and TS2), bridging site over the Cu-Cu bond (bridge) and high-hcp site (h-hcp). All energies are scaled with respect to the energy at l-hcp site.

Supporting information (SI10)

a)

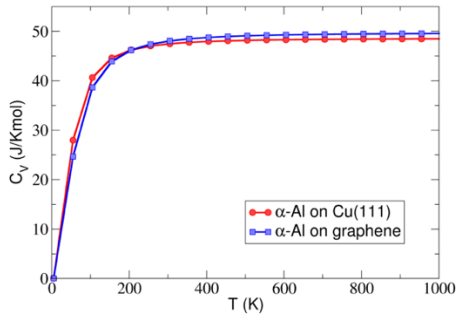

b)

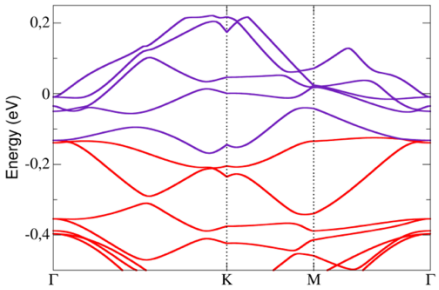

c)

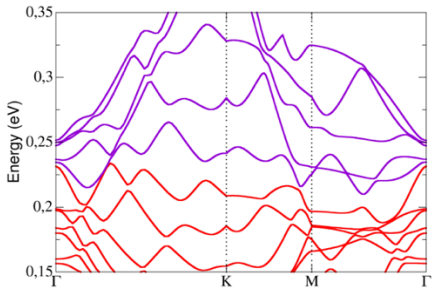

Figure S10. (a) Specific heat (phonon contribution) of α-Al obtained on Cu(111) and graphene substrates at temperatures up to 1000 K. The values converge to similar values of 47.48 J/Kmol on Cu(111) and 48.06 J/Kmol on graphene at room temperature. This is expected since aluminene is structurally very similar on Cu(111) and on graphene. Electronic band structure of (b) α-Al/graphene and (c) α-Al/Cu(111) systems with closed band gap. Valence bands are coloured red, while conduction bands are coloured violet.

References

1. C. G. Broyden, The Convergence of a Class of Double-Rank Minimization Algorithms. *J. Inst. Math. Its Appl.*, 1970, **6**, 76-90.
2. Ch. Tan, Q. Yang, R. Meng, Q. Liang, J. Jiang, X. Sun, H. Ye, X. P. Chen, An AlAs/germanene heterostructure with tunable electronic and optical properties via external electric field and strain. *J. Mater. Chem. C*, 2016, **4**, 8171-8178.
3. G. Wang, R. Pandey, S. P. Karna, Atomically Thin Group V Elemental Films: Theoretical Investigations of Antimonene Allotropes. *ACS Appl. Mater. Interfaces*, 2015, **7**, 11490–11496.
4. Q. Wei, X. Peng, Superior mechanical flexibility of phosphorene and few-layer black phosphorus. *Appl. Phys. Lett.*, 2014, **104**, 251915.
5. N. J. Roome, J. D. Carey, Beyond Graphene: Stable Elemental Monolayers of Silicene and Germanene. *ACS Appl. Mater. Interfaces*, 2014, **6**, 7743−7750.